XLVI CILAMCE
VITÓRIA - ES - BRAZIL - 2025
XLVI IBERO-LATIN AMERICAN CONGRESS ON COMPUTATIONAL METHODS IN ENGINEERING

Revisiting the *fib* blind competition: insights into the numerical modeling of steel-fiber reinforced concrete beams

Lucas Teotônio de Souza[1,2], Pierre Rossi[1], Eduardo de Moraes Rego Fairbairn[1], Michèle Schubert Pfeil[1]

[1]*COPPE, Civil Engineering Program, Universidade Federal do Rio de Janeiro*
Centro de Tecnologia–Bloco I–Sala I216, Ilha do Fundão, CEP 21945-970, Rio de Janeiro/RJ, Brazil
lucas.souza@coc.ufrj.br, pierre.rossi@coc.ufrj.br, eduardo@coc.ufrj.br, mpfeil@coc.ufrj.br
[2]*Núcleo de Construções Civis, Instituto Federal do Sudeste de Minas Gerais*
Rua Bernardo Mascarenhas, 1283, Fábrica, CEP 36080-001, Juiz de Fora/MG, Brazil
lucas.teotonio@ifsudestemg.edu.br

Abstract. The second blind simulation competition (BSC) organized by the *fib* WG 2.4.1. took place in 2021 proposing the numerical modeling of a hybrid fiber reinforced concrete (R/FRC) shallow beam to assess the predictive performance of FEM-based computational models on the design verification at serviceability and at ultimate limit state conditions (SLS and ULS, respectively). This work revisits this benchmark aiming to address two issues not detailed in the BSC. The commercial finite element software DIANA is the chosen numerical tool, in which a classical smeared crack model is used to simulate the FRC properties and bar elements to represent the longitudinal reinforcement. It is shown that the modeling of the steel/FRC bond plays as important role in the structural behavior at SLS. It also discusses the influence of the modeling of the FRC compressive properties on the structural behavior at ULS by applying three different curves. The better correlation between the numerical results and the 2nd BSC experimental tests are obtained by using the parabolic compression curve for the FRC and the no-failure bond-slip interface model for the steel/FRC connection.

Keywords: Fiber Reinforced Concrete (FRC), Hybrid Fiber Reinforced Concrete (R/FRC), Modelling of the Steel/FRC Bond, Blind Simulation Competition (BSC), Finite Element Method.

1 Introduction

Steel fibers contribute significantly to crack control in fiber-reinforced concrete (FRC) constructions, as demonstrated by consolidated research in the literature (Rossi [1]; Rossi and Harrouche [2]; Rossi, Acker and Malier [3], Andrade *et al.* [4]). The combination of fibers with reinforcing bars, known as hybrid reinforcement, significantly improves the structural behavior. This positive contribution of the fibers is related to their action on a different scale from that of the concrete cracking process while complementing conventional reinforcement (Rossi [1]).

The Finite Element Method (FEM) has been applied to evaluate the cracking process and the global behavior of concrete structures (Rossi [5]; Rita *et al.* [6]). Concrete cracking models implemented in commercial computer codes are mostly based on smeared crack models (SCM) as found in Zhou and Feng [7], De Borst [8], De Borst and Nauta [9] and Rots *et al.* [10]. However, many errors are encountered in simulation results, making it important to evaluate reliable prediction models (Barros *et al.* [11]).

In this context, the second Blind Simulation Competition (BSC) organized by fib WG 2.4.1 aimed to evaluate the predictive performance of finite element method (FEM)-based models for the analysis and design of hybrid-strengthened structures. The chosen structure was a shallow beam for which two models were tested up to failure. Performed measurements include the applied loads, crack widths, material deformations in critical zones and the overall structural behavior (Barros *et al*. [12]). This work aims to revisit the BSC by demonstrating the influence of steel/FRC connection modeling on in-service structural behavior (SLS) and FRC compressive behavior modeling on ultimate limit state (ULS) structural behavior.

2 The analyzed structure

2.1 Structural scheme

Figure 1 (Barros *et al* [12]) shows the structure considered in the BSC, including details of the support and loading conditions. It is a two equal spans continuous shallow beam subjected to point loads at midspans. The beam has uniform rectangular cross-section and is reinforced with longitudinal bars at the bottom and top (the latter, over the central support). A higher reinforcement ratio is provided in the midspan region, in each span. A concrete cover thickness of 25 mm is adopted. The end supports allow horizontal displacement on the x_1 axis and rotations around x_1 and x_3 axes, while the intermediate support only allows rotation (u_3).

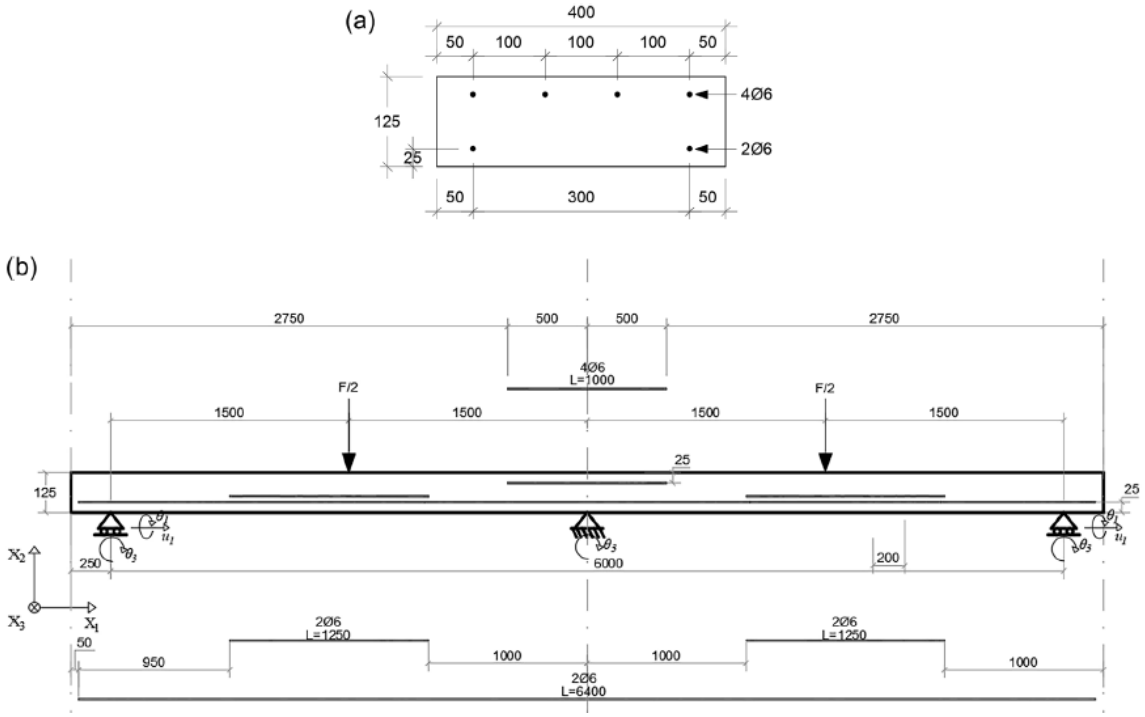


Figure 1 - Geometry of the continuous shallow beam: (a) cross-section; (b) longitudinal view (Barros *et al*. [12])

2.2 Properties of fibers, steel and concrete

Hooked end steel fibers with 1900 MPa tensile strength were used with the following geometric properties: length equal to 60 mm, diameter equal to 0.9 mm. The steel bars for the beams' flexural reinforcement are 6 mm in diameter and have a ribbed surface, with modulus of elasticity, yield stress, and tensile strength respectively equal to 222,199, 627.25, and 769.57 MPa, with standard deviations of 14,970, 15.41, and 13.27 MPa.

The FRC properties were determined at 19 days. The density of the concrete is equal to 2387 kg/m³. The compressive strength and modulus of elasticity are shown in Table 1 (mean and standard deviation). Three-point bending tests with notched beams were performed to evaluate the residual flexural tensile strength parameters ($f_{R,1}$, $f_{R,2}$, $f_{R,3}$, $f_{R,4}$, presented in Table 1, which correspond to the crack opening displacement, CMOD, of 0.5, 1.5, 2.5 and 3.5 mm, respectively).

Table 1 – FRC properties at 19 days of age: average compressive strength (f_{cm}), secant modulus of elasticity in compression (E_{cm}); proportionality limit ($f_{f,Lm}$) and residual flexural strengths ($f_{R,im}, i = 1$ to 4) (standard deviation values in MPa).

Situation	Compression		Bending				
Property	f_{cm}	E_{cm}	$f_{f,L}$	$f_{R,1m}$	$f_{R,2m}$	$f_{R,3m}$	$f_{R,4m}$
Value (MPa)	57.8 (1.0)	31900 (400)	5.3 (0.6)	6.2 (1.5)	7.4 (1.4)	7.6 (1.4)	7.3 (1.1)

3 Numerical model in DIANA

The finite element model was constructed in the commercial software DIANA FEA [13] in a two-dimensional configuration, with plane stress elements for the concrete and embedded truss elements for the longitudinal reinforcement. Due to the symmetry of the structure, as seen in Fig. 1b, only the left half of the beam was modeled.

3.1 Model geometry and boundary conditions

The model was divided into four geometric shapes: beam, load plate, left support plate, and right support plate (representing half of the beam's central support). The flexural reinforcement is modeled as bars located at the level of their centroidal axis. The left half of the beam is 3250 mm long and 125 mm high; the dimensions of the load plate and the right support plate are 40 x 60 mm, and of left support plate, 80 x 60 mm. The upper reinforcement sections were designated Bar4M6-500, representing four 6.0 mm rebars with 500 mm length. The lower reinforcement section was divided into three parts, from left to right: Bar2M6-950, Bar4M6-1250, and Bar2M6-1000, comprising two 6.0 mm bars with 950 mm length, four 6.0 mm bars with 1250 mm length, and two 6.0 mm bars with 1000 mm length, respectively.

To represent the boundary conditions, translation in the Y direction is prevented at the midpoint of the supports and load plates, in addition to translation in the X direction of the right-hand support. Due to the symmetry condition, translation in the X direction is prevented at the beam's symmetry edge. Figure 2 shows the geometry and boundary conditions of the model.

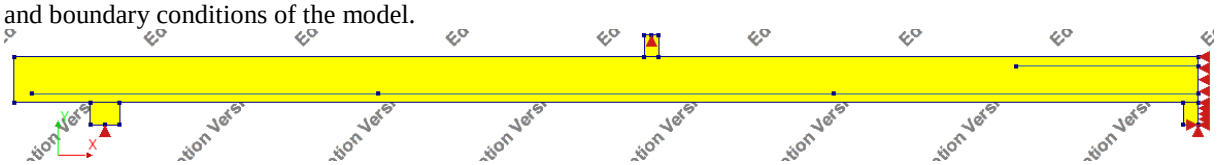


Figure 2 – Complete geometry and boundary conditions of the model.

3.2 Fiber concrete modeling

The FRC response was simulated using the smeared crack model (Rots *et al.* [10]), by means of the rotational crack orientation search method (Rots and Blaauwendraad [14]). The material mechanical properties are those depicted in Section 2.2.

The compression behavior was initially defined by the parabolic curve, with a compression fracture energy of 35,975 N/mm, like that proposed by DIANA Tutorial [15]. After evaluating the various models for the behavior at the steel-concrete interface, the influence of the following compression curves on the ULS behavior of the beam is studied: parabolic, Hognestad parabola and CEBFIB.

3.3 Modeling of the flexural reinforcement and the steel-concrete interface behavior

The mechanical properties considered for the reinforcement are described in Section 2.2. The nonlinear Von Mises plasticity model without hardening is adopted for the rebars constitutive law in tension. The bond-slip model at the steel-concrete interface is applied with a normal modulus of rigidity equal to 100,000 N/mm³ and a shear modulus of rigidity of 100 N/mm³, like that proposed by DIANA Tutorial [16].

The modeling of the steel-concrete interface influences the structural behavior of the beam in SLS. To evaluate this influence, six failure models at the steel-concrete interface were tested with parameters available in the DIANA Tutorial [16]: No Failure Bond-slip Interface, Cubic Function (Dorr), Power Law (Naokowski), Shima Bond-slip Relation, Shima Bond-slip-strain Relation and fib Model Code for Concrete Structures 2010. It should be noted that, for these situations, the compression behavior of the concrete was represented by the parabolic curve.

3.4 Additional model characteristics: steel plates, interfaces, loading and mesh type

The supporting and loading steel plates were modeled in a linear-elastic regime with a modulus of elasticity of 210,000 N/mm², Poisson's ratio of 0.3, and no mass. Interface elements were defined between the steel plates and the beam to ensure adequate connection between the elements, transferring the imposed loads and displacements. The element class is "Structural Interfaces," with properties obtained from Belletti *et al.* [17]: 2D line interface element type; normal rigidity modulus in the Y direction of 34,200 N/mm³; shear rigidity modulus in the X direction of 3.42 x 10^{-4} N/mm³.

The loading was applied as a prescribed translational displacement in the Y direction with a value of -0.1 mm at each loading step. The mesh applied to the beam and support and loading plates is composed of quadrilateral elements with a size of 12.5 mm. The adaptive element size was considered, with a transition smoothness equal to 0.5. Figure 3 shows the mesh applied to the beam under analysis.

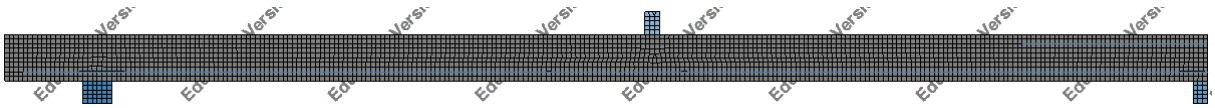


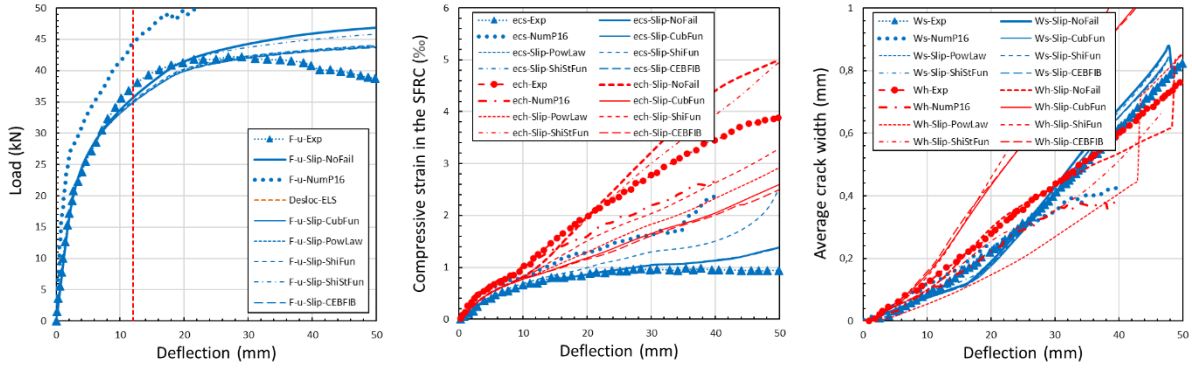
Figure 3 – Mesh applied to the beam under analysis.

4 Results and discussion

The numerical results obtained in this work are compared with the experimental results of the BSC and with the numerical responses of Participant 16 (P16), who achieved the best crack width prediction. The P16 used discrete crack model (DCM) and in-house software. Among the 18 groups in the BSC, 13 used SCM, 2 DCM, and 3 other models. Furthermore, 12 modeled in commercial software and 6 in-house software.

4.1 Influence of steel-concrete connection modeling on the structural behavior

Figure 4 presents the results for six models of the steel-concrete interface available in the DIANA literature: No Failure Bond-Slip Interface, Cubic Function (Dorr), Power Law (Naokowski), Shima Bond-Slip Relation, Shima Bond-Slip-Strain Relation, and fib Model Code for Concrete Structures 2010. Fig. 4b shows that the compressive strain in the FRC is the most affected response, followed by the crack width (Fig. 4c). On the other hand, the overall behavior of the beam changes less with the different models (Fig. 4a). Note that among the simulated cases, the responses that most closely resembled the tests were obtained with the No Failure Bond-slip Interface (Slip-No-Fail) model, which are further discussed in Section 4.3.

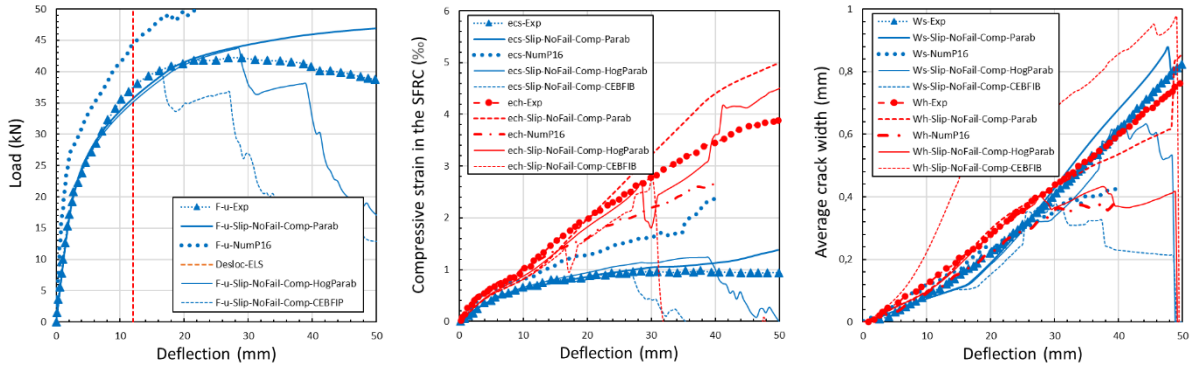


(a) (b) (c)

Figure 4 – Evaluation of the influence of the modeling of the steel-FRC connection on the structural behavior: (a) midspan deflection versus total load ($u - F_t$); (b) midspan deflection versus compressive strain in the FRC at the loaded section ($u - \varepsilon_{c,S}$) and over the intermediate support ($u - \varepsilon_{c,H}$); (c) midspan deflection versus average crack width in the sagging region ($u - w_S$) and in the hogging region ($u - w_H$), at the level of the corresponding tensile reinforcement.

4.2 Influence of the modeling of concrete compressive behavior

Figure 5 presents the responses obtained with different compression curves of FRC: parabolic, Hognestad parabolic, and CEBFIB. The overall behavior of the beam (Fig. 5a), the compression strain in the FRC (Fig. 5b), and the crack width measurement (Fig. 5c) are significantly affected by the concrete compression curve, especially in the ULS. The responses that most closely resemble those of the experiment are those of the parabolic curve, for which further discussion is presented in Section 4.3, along with the No Failure Bond-Slip Interface model.



(a) (b) (c)

Figure 5 – Evaluation of the influence of the concrete compression curve on the structural behavior: (a) midspan deflection versus total load ($u - F_t$); (b) midspan deflection versus compressive strain in the FRC at the loaded section ($u - \varepsilon_{c,S}$) and over the intermediate support ($u - \varepsilon_{c,H}$); (c) midspan deflection versus average crack width in the sagging region ($u - w_S$) and in the hogging region ($u - w_H$), at the level of the corresponding tensile reinforcement.

4.3 Structural behavior with parabolic compression curve and no-failure bond-slip interface

Figure 6a shows a comparison between the deflection versus total load ($u - F_t$) obtained with the DIANA program, the result of Participant 16 of the BSC, and the average deflection experimentally obtained for the two beams. In the tests, the average maximum total load was 42.26 kN and occurred at a deflection of 28.3 mm. For the same experimental deflection of 28.3 mm, 43.83 kN load was obtained in DIANA, and P16 obtained approximately 52.07 kN.

Figure 6b shows a comparison of the relationship between midspan deflection and average crack width for beam 2 (the experimental data for beam 1 was lost) in the loading and central support sections at the level of the tensile reinforcement ($u - w_S/w_H$) with the numerical values from DIANA and P16. According to fib Model Code [18], the deflection under SLS conditions ($u - SLS$) is L/250 = 12 mm, where L is the span between supports. At this deflection, the average crack width in the central support and loading sections was 0.16 and 0.11 mm, respectively, which are smaller than the maximum recommended for aggressive environmental conditions. In the DIANA program, the values obtained were 0.13 and 0.90 mm, while P16 obtained 0.13 and 0.11 mm, respectively.

Figure 6c shows the relationship between deflection and strain in the longitudinal tensile reinforcement in the loading and central support sections ($u - \varepsilon_{s,S}/\varepsilon_{s,H}$). Considering the corresponding average curves and taking into account the adopted reinforcement yield strain ($\varepsilon_{sy} = 2.56$ ‰), the deflection when the reinforcement in the central support and loading sections began to yield was 3.98 and 14.40 mm, respectively. In the DIANA program, the values obtained were 49.0 and 14.38 mm, while P16 obtained 9.05 and 11.62 mm, respectively.

Figure 6d shows the relationship between deflection and compressive strain in the FRC in the loaded section and on the central support, $u - \varepsilon_{c,S}/\varepsilon_{c,H}$. The average experimental values obtained for $\varepsilon_{c,H}$ and $\varepsilon_{c,S}$ at the SLS deflection (12 mm) were, respectively, 1.21 and 0.69 ‰. In this order, the numerical values of the model in DIANA are 0.99 and 0.68 ‰ and 1.11 and 0.89 ‰ for P16. It is found that, in u-SLS, the maximum compressive strains in the respective sections were much smaller than the strain in the FRC compressive strength (ε_{c0}). However, at peak load, the maximum compressive strain in the FRC in the intermediate support region significantly exceeded ε_{c0}, while in the bowing region it was kept almost constant above 24 mm, but much smaller than ε_{c0}.

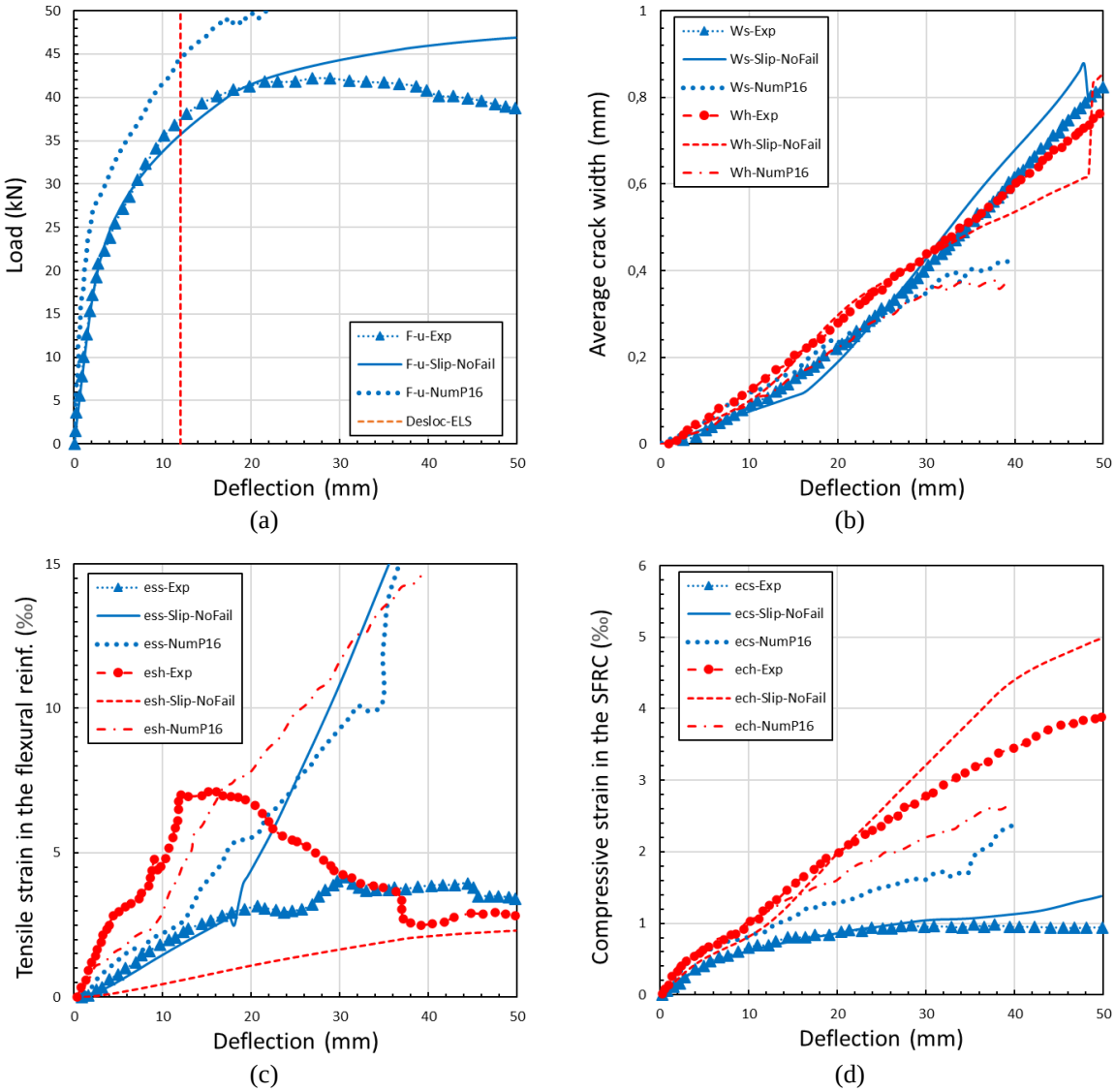


Figure 6 – Comparison of experimental and numerical results from DIANA and P16 of the BSC: (a) midspan deflection versus total load ($u - F_t$); (b) midspan deflection versus average crack width in the sagging region ($u - w_S$) and in the hogging region ($u - w_H$), at the level of the corresponding tensile reinforcement; (c) midspan deflection versus tensile strain in the flexural reinforcement at the loaded section ($u - \varepsilon_{s,S}$) and over the intermediate support ($u - \varepsilon_{s,H}$); (d) midspan deflection versus compressive strain in the FRC at the loaded section ($u - \varepsilon_{c,S}$) and over the intermediate support ($u - \varepsilon_{c,H}$).

Figure 7 shows a comparison of the crack pattern immediately before rupture obtained in this study and by Participant 16, where a good visual correlation between the crack patterns can be noted. It should be noted that, for the DIANA model, the crack scale ranges from 0.00 to 1.55 mm.

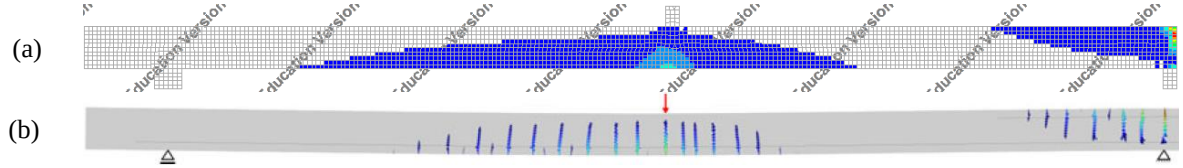


Figure 7 - Crack pattern obtained by: (a) DIANA Program and (b) Participant 16.

5 Conclusion

The predictive performance of FEM-based models for the analysis and design of hybrid-strengthened structures is strongly influenced by the modeling of the steel/FRC connection in the structural in-service behavior (SLS) and the modeling of the FRC compressive behavior in the structural ultimate limit state (ULS). The 2nd BSC requested participants to report on the adopted concrete cracking model but did not consider the compression curve used or the behavior of the steel-concrete interface. For the same structure, this study obtained a better correlation of the numerical responses with the 2nd BSC tests, using the parabolic compression curve for the FRC and the no-failure bond-slip interface model for the steel/FRC connection.

Acknowledgements. This work was carried out with the support of the Instituto Federal do Sudeste de Minas Gerais and the Coordenação de Aperfeiçoamento de Pessoal de Nível Superior - Brazil (CAPES) - Code 001.

Authorship statement. The authors hereby confirm that they are the sole liable persons responsible for the authorship of this work, and that all material that has been herein included as part of the present paper is either the property (and authorship) of the authors or has the permission of the owners to be included here.

References

[1] P. Rossi, "Lés Betons de Fibres". *Editions Martialis*. ISBN 978-2-9577424-0-0, 2021.
[2] P. Rossi and N. Harrouche, "Mix design and mechanical behavior of some steel-fiber-reinforced concretes used in reinforced concrete structures". *Material Structures* 23, 256–266, 1990.
[3] P. Rossi, P. Acker and Y. Malier, "Effect of steel fibres at two different stages: The material and the structures". *Material Structures* 20, 436–439, 1987.
[4] R. G. M. Andrade, M. S. Pfeil, R. C. Battista, R. D. Toledo Filho, O. M. O. Araújo and R. T. Lopes, "Comparison between methods to determine the fiber orientation factor of an HPFRC bridge box girder". *Construction and Building Material*, 2021.
[5] P. Rossi, "Numerical Designing of Fiber Reinforced Concrete Eco-Constructions". *Materials Research*, v. 16, p. 2576, 2023.
[6] M. R. Rita, J-L. Tailhan, E. M. R. Fairbairn, P. Rossi and A. B. C. G. Silva, "A Probabilistic Semi-Explicit Cracking Model for Fiber-Reinforced Concretes". *5th International RILEM Conference on Numerical Modeling Strategies for Sustainable Concrete Structures*, SSCS, 2025.
[7] X. Zhou and B. Feng, "A smeared-crack-based field-enriched finite element method for simulating cracking in quasi-brittle materials". *Theoretical and Applied Fracture Mechanics* 124, 103817, 2023.
[8] R. De Borst, "Computational aspects of smeared crack analysis. In Computational Modelling of Reinforced Concrete Structures". *Pineridge Press*, Swansea, UK, 1986.
[9] R. De Borst and P.Nauta, "Nonorthogonal cracks in a smeared finite element model". *Eng. Comput*. 2, 35–46, 1985.
[10] J. Rots, P. Nauta, G. Kusters and J. Blauwendraad, "Smeared crack approach and fracture localization in concrete". *Heron* 30:1–48, 1985.
[11] J. A. O. Barros *et al.*, "Blind competition on the numerical simulation of steel fibre reinforced concrete beams failing in shear". *fib Structure Concrete Jornal*, 22(2):939–67, 2021.
[12] J. A. O. Barros *et al.*, "Blind competition on the numerical simulation of continuous shallow steel-fiber reinforced concrete beams failing in bending", *fib Structure Concrete Jornal*, vol. 24, no. 3, pp. 1–31, 2023.
[13] DIsplacement ANAlyzer - DIANA - Advanced Finite Element Analysis, 2025.
[14] J. Rots and J. Blaauwendraad, "Crack models for concrete: discrete or smeared? Fixed, multi-directional or rotating?" *Heron*, 34 (1), pp. 1-59, 1989.
[15] DIANA Tutorial, "Reinforced concrete beam: simulation of an experimental test". In: https://dianafea.com/tutorial/reinforced-concrete-beam-simulation-of-an-experimental-test/
[16] DIANA Tutorial, "Bond-slip models in DIANA". In: https://dianafea.com/tutorial/bond-slip-models-in-diana/
[17] B. Belletti, C. Damoni, M. A. N. Hendriks, and A. De Boer, "Validating the Guidelines for Nonlinear Finite Element Analysis of Concrete Structures." *Rijkswaterstaat Technisch Document*. RWS GPO, Utrecht, Netherlands, rtd 1016-2, 2016.
[18] Fib Model Code. Fib Model Code for Concrete Structures, 2010.